3. J. C. Comiso, *J. Clim.* **13**, 1674 (2000).
4. P. T. Doran *et al.*, *Nature* **415**, 517 (2002).
5. The mean near-surface warming was computed from the Climate Research Unit, University of East Anglia, UK database of in situ surface meteorological observations (see www.cru.uea.ac.uk/ftpdata/tavegl2v.dat).
6. J. Turner, J. C. King, T. A. Lachlan-Cope, P. D. Jones, *Nature* **418**, 291 (2002).
7. S. C. B. Raper, T. M. L. Wigley, P. R. Mayes, P. D. Jones, M. J. Salinger, *Mon. Weather Rev.* **112**, 1341 (1984).
8. T. H. Jacka, W. F. Budd, *Ann. Glaciol.* **27**, 553 (1998).
9. J. Turner *et al.*, *J. Clim.* **17**, 2890 (2004).
10. J. K. Angell, *Geophys. Res. Lett.* **26**, 2761 (1999).
11. J. K. Angell, in *Trends Online: A Compendium of Data on Global Change* (Carbon Dioxide Information Analysis Center, Oak Ridge National Laboratory, U.S. Department of Energy, Oak Ridge, TN, 2005); (http://cdiac.esd.ornl.gov/trends/temp/angell/angell.html).
12. P. W. Thorne *et al.*, *J. Geophys. Res.* **110**, 10.1029/2004JD005753 (2005).
13. Angell gives temperature trends for various latitude bands (*10*, *11*) but not a value for 0° to 60°S. Therefore, we calculated it from his values for 0° to 90°S (0.10) and 60° to 90°S (0.29) using the area weighting of 1/6 for 60 to 90°S that Angell uses: 0-60_trend = [0.1 − 1/6 × (0.29)]/5/6, giving a value of 0.06.
14. G. J. Marshall, *J. Clim.* **16**, 4134 (2003).
15. D. H. Bromwich, R. L. Fogt, *J. Clim.* **17**, 4603 (2004).
16. We used the updated version 5.2 of the Temperature of the Lower Troposphere product of the Microwave Sounder Unit in (*24*).
17. R. E. Swanson, *Geophys. Res. Lett.* **30**, 2040 (2003).
18. S. J. Sherwood, J. Lanzante, C. Meyer, *Science* **309**, 1556 (2005).
19. J. K. Luers, R. E. Eskridge, *J. Clim.* **11**, 1002 (1998).
20. D. J. Gaffen, *J. Geophys. Res.* **99**, 3667 (1994).
21. R. Lund, J. Reeves, *J. Clim.* **15**, 2547 (2002).
22. H. B. Bluestein, *Observations and Theory of Weather Systems*, vol. 2 of *Synoptic-Dynamic Meteorology in Midlatitudes* (Oxford Univ. Press, Oxford, 1993).
23. C. Gordon *et al.*, *Clim. Dyn.* **16**, 147 (2000).
24. R. W. Spencer, J. R. Christy, *J. Clim.* **5**, 858 (1992).
25. We are grateful to the Scientific Committee on Antarctic Research for funding the digitization of the Russian radiosonde data.

21 October 2005; accepted 24 February 2006
10.1126/science.1121652

Changes in Surface Water Supply Across Africa with Predicted Climate Change

Maarten de Wit* and Jacek Stankiewicz

Across Africa, perennial drainage density as a function of mean annual rainfall defines three regimes separated by threshold values of precipitation. This nonlinear response of drainage to rainfall will most seriously affect regions in the intermediate, unstable regime. A 10% decrease in precipitation in regions on the upper regime boundary (1000 millimeters per year) would reduce drainage by 17%, whereas in regions receiving 500 millimeters per year, such a drop would cut 50% of surface drainage. By using predicted precipitation changes, we calculate that a decrease in perennial drainage will significantly affect present surface water access across 25% of Africa by the end of this century.

Water is essential to human survival, and changes in its supply from overland flow can potentially have devastating implications, particularly in Africa, where much of the population relies on local rivers for water. Future climate change poses one of the greatest threats to poverty eradication on this continent, and related changes in surface water supply will exacerbate this threat (*1*). To predict future supply, it is necessary to understand how the drainage relates to biological, geological, and atmospheric parameters. These form a highly complex system, but simpler relationships can be identified within it, in particular relating drainage to precipitation. Even this relationship is nonlinear (*2*, *3*). Our detailed analysis of the African river systems identifies three climatic regimes. Areas receiving a low rainfall have virtually no perennial drainage. Above a threshold rainfall, there exists an intermediate range in which the drainage density increases with increasing rainfall. This regime can be termed "unstable": A change in climate would directly result in a change in surface water supply. This relationship is not indefinite; in high-rainfall areas other factors, like vegetation, begin to play a role, and a slight decrease in drainage density with increasing rainfall is observed. Here, we quantify how a moderate but variable change in precipitation across Africa by the second part of this century, as predicted by an ensemble of global climate-change models, would directly affect African countries, 75% of which fall at least partially into the unstable intermediate rainfall regime.

Our studies make use of AEON's Africa Database (*4*). This geographic information system (GIS) database includes all rivers and lakes in Africa (Fig. 1), manually digitized from topographic maps of individual countries on the basis of their own cadastral databases (figs. S1 to S4). The average stream separation (ratio of land area to total stream length) of the set is 15 km. This corresponds to about 2 million km of digitized rivers. Streams were checked against the 90-m SRTM (Shuttle Radar Topography Mission) digital elevation model (DEM) and were found to be within 300 m from valleys seen on the DEM. This uncertainty is two orders of magnitude less than the resolution of the database. All streams have also been classified as either perennial or nonperennial (as defined on local cadastral maps), and all river networks were ordered according to the Horton-Strahler ordering scheme (*5*). The database also includes climatic conditions over the African continent, such as seasonal rainfall and temperatures (*6*).

To understand the relationship between rainfall and drainage in Africa, we did a continental scale analysis by subdividing Africa into square blocks of 1000 km across [giving areas of 1,000,000 km^2; smaller areas near the coast were combined into bigger blocks (Fig. 1 inset)]. For each of the 37 blocks, we computed the mean annual precipitation as well as the perennial drainage density. This latter quantity is the total perennial stream length per unit area. The exact value of the total length, and thus of the density, depends on the resolution of the map from which the streams were obtained. There are also many finer points of what exactly constitutes a stream (*2*, *4*, *7*). For this reason, it is meaningless to compare density values from different studies on other continents, for example, unless the same resolution and standardized parameters are used. It is also important that these parameters are constant throughout the analysis; otherwise density variations could be observed where none really exist. The plot of perennial density as a function of mean annual precipitation is shown in Fig. 2A. A similar regional analysis was done for southern Africa (south of the Zambezi river, Fig. 1). Here, 24 blocks 500 km across were used (figs. S1 and S2), and the observed results are shown in Fig. 2B.

From the plots in Fig. 2, perennial drainage density as a function of mean annual rainfall consists of regimes separated by threshold values of precipitation. Areas receiving less than 400 mm year^{-1} have almost no perennial drainage (*8*). Above this threshold of ~400 mm year^{-1}, the perennial drainage density initially increases with increasing precipitation, but this does not go on indefinitely. The next threshold is defined statistically at ~1000 mm year^{-1} (*9*).

We therefore propose a model for the relationship between mean annual precipitation and perennial drainage that comprises three scaling regimes separated by two thresholds. Areas receiving less than 400 mm year^{-1} have no perennial drainage, unless they are mountainous regions conducive to runoff (*8*). Above that threshold, density increases linearly with increasing precipitation until another threshold of ~1000 mm year^{-1} is reached. Above that value, the density decreases slightly with increasing rainfall (*8*). We do not know whether there is

Africa Earth Observatory Network (AEON) and Department of Geological Sciences, University of Cape Town, Rondebosch 7701, South Africa.

*To whom correspondence should be addressed. E-mail: maarten@cigces.uct.ac.za

another threshold and a fourth regime for even higher rainfall, but the three-regime model covers the precipitation range of Africa adequately. Some implications of the model summarized in Fig. 2 are shown in Fig. 3A, whereas Fig. 3B shows the distribution of the three rainfall regimes across Africa. The dry regime (marked in red) covers the largest area (41% of the continent), but the intermediate regime (marked in yellow; ~25% of Africa) is of most interest here, because this is where changes to precipitation would result in serious changes in drainage supply. Two densely populated regions are of particular concern. First, southern Africa is in a very disturbing situation. Most of it falls into the unstable regime, and large sections of the arid regime receive their only water from the Orange River, with its sources in the unstable areas. Second, most of East Africa is also in the intermediate range, as are large sections of the upper Nile.

With our model, we now attempt a prediction of the perennial water supply across Africa by the end of this century. That human impact is a major driving force behind the climate changes in the last century is accepted by most scientists [see, for example, (*1*, *10*–*12*)]. Global warming due to anthropogenic emission of greenhouse gasses has received more attention from scientists than can be referenced here. In a recent presentation (*13*), Anthony Nyong said that Africa risks bearing the brunt of this climate change unless urgent action is taken now. He estimated that by year 2050 rainfall in sub-Saharan Africa could drop by 10%, leading to major water shortages. A 10% decrease in precipitation in regions on the intermediate regime's upper boundary (1000 mm year^{-1}) would reduce drainage by 17%, whereas in regions receiving 500 to 600 mm year^{-1} such a drop would cut 50 to 30%, respectively, of surface drainage (Fig. 3A). However, a uniform climate change on a continental scale is clearly a gross simplification, and we use a more detailed future rainfall estimate across Africa as summarized below.

We first make use of the results of the climate change assessment project for Africa by the Climate System Analysis Group (CSAG) based in Cape Town, South Africa (*14*). This group uses results from six global circulation models (GCMs) to assess the projected changes in mean annual rainfall across Africa for the past three decades of the 21st century and to downscale these to regional scales of relevance (*15*, *16*). The GCM simulations span the 20th century with use of specified anthropogenic forcing and continue through the 21st century by using the special reports on emission scenarios (SRES) of increasing greenhouse gas emissions (*17*). Detailed discussion of the configuration of each model simulation is beyond our scope, and the interested reader is referred to the research groups responsible for each model (*14*, *18*–*24*). We follow the example of the CSAG by using the average forecast of these models for Africa and the range covered by the models as a measure of uncertainty. In addition, we compare these forecasts to a composite ensemble of African precipitation models for the period 2070 to 2099, derived from 21 fully coupled ocean-atmosphere GCMs listed by the Intergovernmental Panel on Climate Change (IPCC) (*24*–*26*).

One input parameter used in all the models that will be mentioned is the anthropogenic

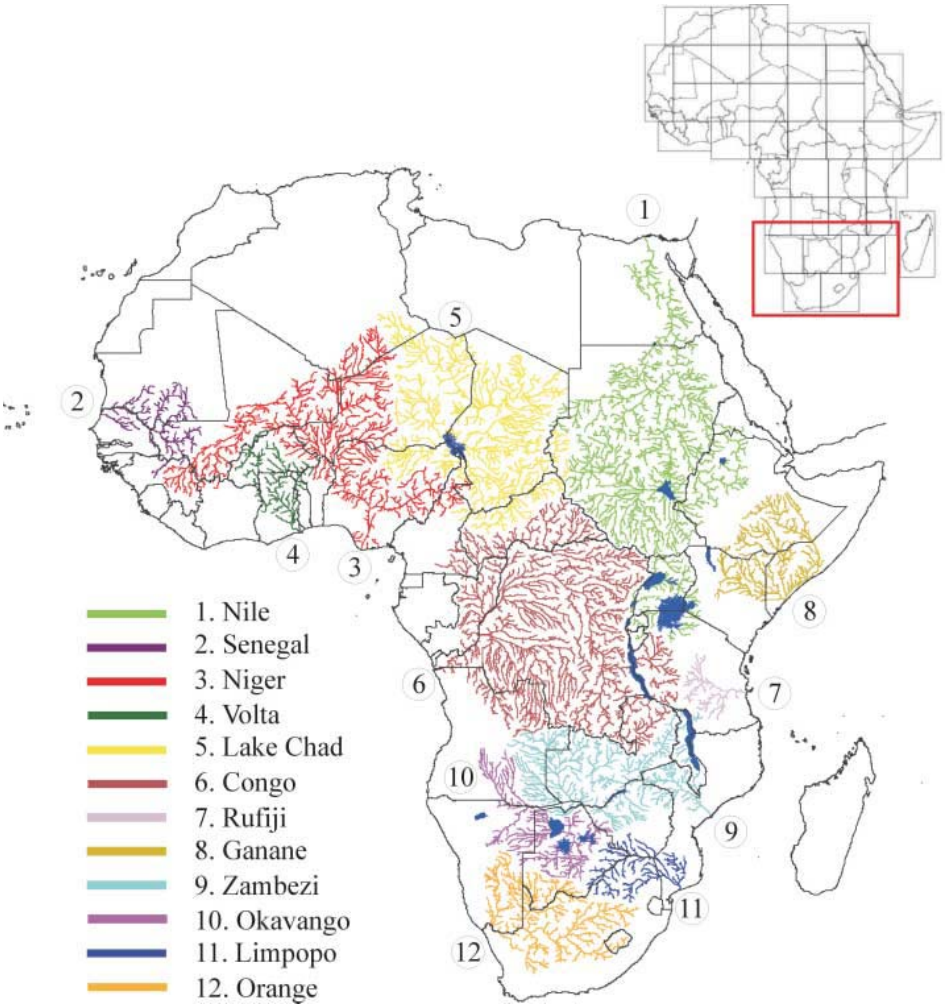

Fig. 1. Major river basins in Africa, selected from the AEON Africa Database. This is not the full resolution of the database. More detailed examples can be viewed in figs. S1 to S4. (**Inset**) 37 Africa-wide blocks (black lines) used to study the relationship between rainfall and drainage. Red block marks southern Africa, which was subdivided into 24 blocks (figs. S1 and S2).

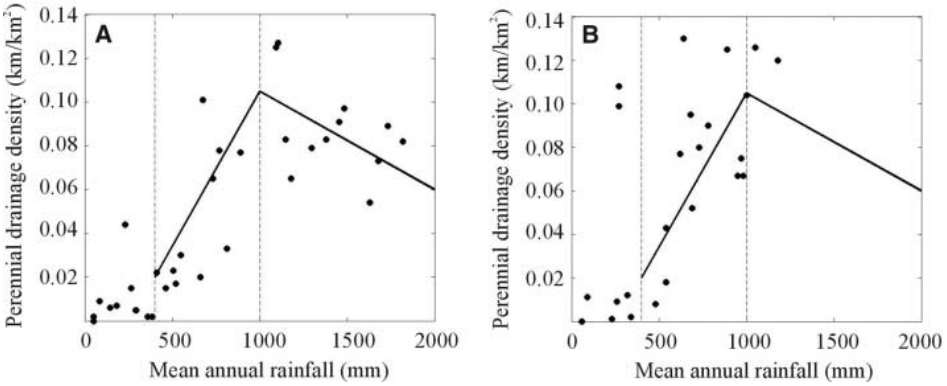

Fig. 2. Perennial drainage density as a function of mean annual rainfall, measured for individual blocks for the whole of Africa (**A**) and southern Africa (**B**). Dashed vertical lines show thresholds of 400 and 1000 mm year^{-1}. Black lines show best linear fits of the combined data sets inside the intermediate and high rainfall regimes (*9*).

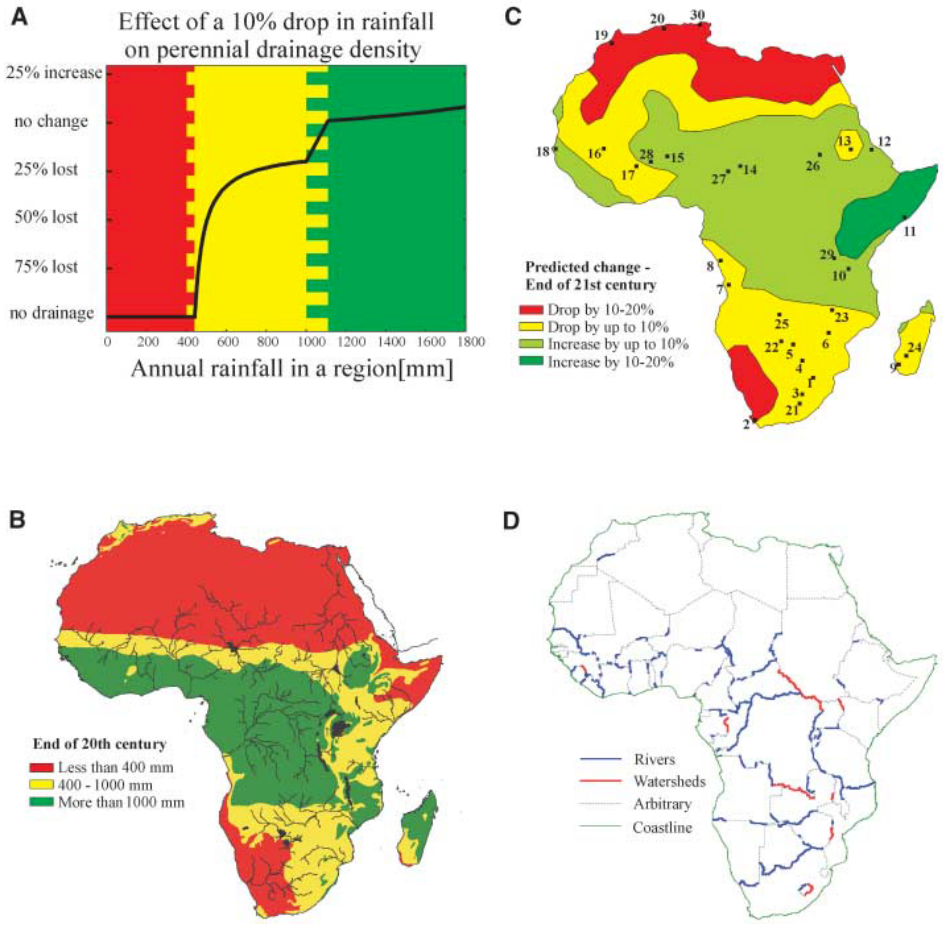

Fig. 3. (**A**) Graph showing the implications of our rainfall–perennial drainage density model. Black curve shows what change in perennial drainage would occur in a region if annual precipitation dropped by 10%. This curve is a function of the annual drainage in the region before the change. The three colors correspond to the three rainfall regimes, distribution of which is shown in (B). The two zippers show rainfall ranges where a 10% drop resulted in crossing a threshold. Regions receiving between 401 and 444 mm year^{-1} would drop under 400 (from yellow to red in our color scheme), and those receiving between 1001 and 1111 mm year^{-1} would go from the green to the yellow. One of the consequences of the observed relationship between rainfall and drainage is that a small change in precipitation in a region in the intermediate, unstable regime can cause substantial changes in the perennial water supply. If, for example, in a region receiving 600 mm year^{-1} of rain, the precipitation decreases to 550 mm year^{-1} (a change of less than 10%), perennial drainage will be cut by 25%, wheras a change from 500 mm year^{-1} to 450 mm year^{-1} would cut the drainage by half. (**B**) Present rainfall regimes in Africa. Dry areas (receiving not more than 400 mm year^{-1}) are marked in red. These areas make up 44% of the continent's total area (three countries in Africa fall entirely in this region: Egypt, Djibouti, and Saharawi). The intermediate regime (not more than 1000 mm year^{-1}) is marked in yellow (25% of area; affecting at least partially 75% of all African countries), and the high rainfall areas are marked in green (31%). Only the major rivers and lakes have been superimposed on the figure. Not all of these rivers are perennial. (**C**) Simplified map of Africa showing expected change in precipitation by the end of the 21st century on the basis of the composite of 21 leading fully coupled GCMs adapted by the IPCC for forecasting purposes (*14*, *24*). Here, 10% change contours have been used to simplify the figure; the original models are considerably more detailed. Numbers 1 to 30 are selected positions throughout Africa where we have calculated the expected changes in perennial drainage density (Table 1). Points 1 to 20 correspond to urban areas, whereas 21 to 30 represent rural areas. (**D**) International borders in Africa. Of all inland boundaries, rivers form 33% (blue), with another 6% made up by watersheds (red). These river-related borders apply to 39 of the 48 (i.e., 81%) countries on Africa's mainland. Arbitrary inland borders are shown in gray stipples, and the coastline in green.

CO_2 input into the atmosphere to trace its long-term effect on climate change. Depending on how this changes over the years, each model produces different scenarios depending on the time-integrated greenhouse gas emissions (*17*, *24*, *25*). Here, we concentrate on a relatively optimistic model that includes the assumption of a timely and effective development of nonfossil energy supply (the B1 marker scenario, normalized to the historically observed precipitation in Africa for the 20-year period from 1979 to 1998) (*24*, *25*). On the basis of the above model, the mean expected changes in large-scale precipitation across Africa in the last quarter of the 21st century are shown in Fig. 3C.

For further analyses, 30 selected urban and rural areas in Africa lying in the unstable regime are located on Fig. 3C and listed in Table 1. Two-thirds of the data are derived from cities or towns, because rainfall data are less reliable in rural Africa and because city or town data provide reasonable proxies to large surrounding rural regions. The table shows what percentage of today's perennial drainage the area will have after a specific change in precipitation. Four scenarios are considered: decrease by 10% and 20% and increase by the same amounts. The expected scenario (Fig. 3C) is marked with an asterisk, and some are briefly highlighted below.

Most of southern Africa (including southern Madagascar) lies in either the unstable or the dry regime (Fig. 3B), and much of this region is projected to experience significant losses of what little drainage it does have (Fig. 3C). Areas near Cape Town will likely suffer most, losing more than half their perennial supply. This means there will be no relief for this drought-stricken region (*27*). In addition, the eastern and northern section of the subregion are projected to experience strong to moderate decreases in their water supply. Any such loss in eastern South Africa would affect the upper reaches of the Orange River, whose lower reaches are one of few perennial water supplies in southwestern Africa. The interior of this region is very dry, but the Orange River, with its sources in the east, winds its way through the arid region. This is a major river, with a mean annual discharge of over 11,000 km^3, making it the fifth largest river in Africa and one of the 50 largest ones globally (*28*). However, there were at least five instances between 1862 and 1912 (before any damming schemes) of this river running dry (*29*). In 1903 the river stopped flowing for 2 months, showing that even one of the continent's biggest rivers cannot be truly called perennial. Today, western South Africa is experiencing its biggest drought in over 100 years (*27*), and water shortages in central South Africa in late 2004 led to almost no water being released from the dams on the Orange River. This caused the lower reaches of this river, where it forms the border of Namibia, to reach a very low level.

East Africa's future looks better, with increases of drainage density to be expected, because parts of the region may expect an increase in rainfall that could even put it into the wet regime. However, although Somalia's supply (Mogadishu) could go up by a factor of 10, this may not significantly increase its drainage density (e.g., 10 times very little does not necessarily translate to floods), and this may also stretch the limits of interpreting the spatial detail of the GCM results.

Table 1. Percentages of perennial drainage that will remain following a given change in precipitation. Rainfall values (in mm year^{-1}) obtained from (*32*) for cities 1 to 20 and from the CSAG (*14*) station data archive for rural districts 21 to 30. The potential scenario for each locality at the end of this century, based on climate change models discussed in the text, is marked with an asterisk.

No.	City	Country	Rainfall	During	10% Drop	20% Drop	10% Rise	20% Rise
1	Johannesburg	South Africa	723	1951–1990	78%*	55%	122%	145%
2	Cape Town	South Africa	612	1837–1989	71%	42%*	129%	158%
3	Bloemfontein	South Africa	557	1903–1990	65%*	29%	135%	171%
4	Gaborone	Botswana	526	1922–1988	58%*	17%	142%	183%
5	Maun	Botswana	465	1921–1989	28%*	0%	172%	243%
6	Harare	Zimbabwe	830	1890–1989	81%*	61%	119%	139%
7	Catete-Sede	Angola	606	1918–1972	71%*	41%	129%	159%
8	Cabinda	Angola	798	1913–1980	80%*	60%	120%	140%
9	Tulear	Madagascar	420	1951–1990	0%*	0%	310%	520%
10	Dodoma	Tanzania	551	1922–1989	64%	27%	136%*	173%
11	Mogadisu	Somalia	409	1911–1990	0%	0%	554%	1009%*
12	Adi Ugri	Eritrea	642	1899–1976	73%	47%	127%*	153%
13	Gedaref	Sudan	626	1903–1990	72%*	45%	128%	155%
14	Ndjamena	Chad	570	1904–1990	66%	33%	134%*	167%
15	Niamey	Niger	556	1905–1990	64%	29%	136%*	171%
16	Mourdiah	Mali	529	1930–1985	59%*	18%	141%	182%
17	Ouagadougou	Burkina Faso	814	1902–1990	80%*	61%	120%	139%
18	Dakar	Senegal	505	1897–1990	52%	4%	148%*	196%
19	Rabat	Morocco	538	1930–1989	61%	22%*	139%	178%
20	Algiers	Algeria	660	1870–1973	75%	49%*	125%	151%
				Rural districts				
21	Zastron	South Africa	570	1979–2000	66%*	33%	134%	167%
22	Okavango	Botswana	460	1973–2003	23%*	0%	177%	253%
23	Chipata	E. Zambia	840	1979–2000	81%*	62%	119%	136%
24	Isalo-Ihosy	Madagascar	870	1979–2000	81%*	63%	119%	125%
25	Western	W. Zambia	730	1979–2000	78%*	56%	122%	144%
26	S. Kordofan	Sudan	460	1979–2000	23%	0%	177%*	253%
27	Marona	Cameroon	680	1979–2000	76%	51%	124%*	149%
28	Foda Ngourma	Burkina Faso	830	1979–2000	81%	61%	119%*	140%
29	Northwest	Tanzania	670	1979–2000	75%	50%	125%*	150%
30	Jendouba	Tunisia	440	1979–2000	0%	0%*	210%	320%

A third major unstable area, visible in Fig. 3B, is the east-west band stretching from Senegal to Sudan, separating the dry Sahara from wet Central Africa. This band might look unsubstantial, but it crosses a number of important water bodies, such as the Sudd swamps in the Nile Basin, Lake Chad (which has now shrunk to 10% of its size in 1963), and the Niger River on either side of its inland delta (*30*). The predicted evolution of the southern boundary of the Sahara in west Africa appears complex: The desert's limit should move northward in Chad and Niger, but farther west (Burkina Faso and Mali) the desert will continue to spread south. Although this relies on the finer spatial details of the GCMs, none of the IPCC models predicts enough rainfall change to suggest perennial river networks in the Sahara this century or to have any direct effect on Central and West Africa in the wet regime.

Although water storage and management systems in most large cities can be reengineered to cope with most changes in runoff regimes, the results of this study provide African states with an opportunity to focus adaptation responses on those rural areas where the risk of loss of perennial water is high and more likely to create scarcity. But water can also be a source of international conflict. River channels and basin watersheds frequently demarcate international boundaries; in Africa they make up almost 40% of these borders (Fig. 3D). Furthermore, all major African rivers traverse international boundaries. To what extent reduced flow in major rivers reflects direct changes in rainfall-runoff discharge and groundwater flow, rather than reduced perennial drainage as suggested here, requires further study. However, our results indicate that future access to water, especially in rural areas that depend on low-order streams for surface supply, needs to be seriously addressed by countries that share river basins and that the ability to estimate the future water supply, like this study does, is an essential requirement for water basin management throughout the African continent.

References and Notes

1. World Bank *et al., Poverty and Climate Change: Reducing the Vulnerability of the Poor Through Adaptation* (World Bank, Washington, DC, 2003) (http://lnweb18.worldbank.org/ESSD/envext.nsf/46ByDocName/KeyThemesVulnerabilityandAdaptationPovertyandClimateChange).
2. K. J. Gregory, in *Geomorphology and Climate*, E. Derbyshire, Ed. (Wiley, New York, 1976), pp. 289–315.
3. G. E. Moglen, E. A. B. Eltahir, R. L. Bras, *Water Resour. Res.* **34**, 855 (1998).
4. J. M. Stankiewicz, M. J. de Wit, *Geophys. Geochem. Geosyst.* **6**, 10.1029/2005GC000928 (2005).
5. A. N. Strachler, *Eos* **38**, 913 (1957).
6. D. R. Legates, C. J. Willmot, *Int. J. Climatol.* **10**, 111 (1990).
7. D. R. Montgomery, W. E. Dietrich, *Nature* **336**, 232 (1988).
8. Exceptions to this rule are found in mountainous areas, which are conducive to runoff. This factor accounts for the anomalous point showing perennial density of 0.44 km^{-1} at a rainfall of just over 200 mm year^{-1} in Fig. 2A. This point represents the western section of southern Africa. In the south of the block are steep mountain ranges, collectively known as the Cape Fold Belt. The majority of the rainfall in this area is concentrated in these mountains, which causes a number of perennial rivers to form on the southern extremity of Africa. This anomaly can also be seen in Fig. 2B: Two points give perennial density near 0.1 km^{-1} despite receiving just over 200 mm year^{-1}.
9. The precipitation threshold was moved between 600 and 1400 mm year^{-1}, and points combined from both data sets (Fig. 2) were separated by it into two subsets. Correlation coefficients for each subset were computed. The average of the two correlation coefficients is highest when the precipitation threshold was just over 1000 mm year^{-1}. The individual coefficient is 61.7% for regions receiving between 400 and 1000 mm year^{-1} and an inverse correlation of 59.2% for regions receiving above 1000 mm year^{-1}. Both these correlations can be stated with a confidence of 99%. An identical result was obtained using

GraphPad Prism 4 developed by GraphPad Software (*31*). The inverse correlation in the high rainfall regime is probably the result of dense vegetative growth entering the relationship. We do not know how far this wet regime extends; using the regression computed in this study it would intercept the rainfall axis (i.e., the point of no perennial drainage) at 3200 mm year^{-1}, almost twice as much precipitation as our wettest data point.

10. IPCC, *Climate Change 2001,* J. T. Houghton *et al.*, Eds. (Cambridge Univ. Press, Cambridge, 2001).
11. H. von Storch *et al.*, *Science* **306**, 679 (2004).
12. D. A. Stainforth *et al.*, *Nature* **433**, 403 (2005).
13. A. Nyong, abstract in *Impacts of Climate Change in the Tropics: The African Experience. Avoiding Dangerous Climate Change* (Meterological Office, Exeter, UK, 2005) (www.stabilisation2005.com).
14. CSAG, *Assessments of Impacts and Adaptations to Climate Change: Africa Climate Change Scenarios, Volume 1* (2002) (www.csag.uct.ac.za).
15. B. C. Hewitson, R. G. Crane, *Int. J. Climatol.,* in press.
16. B. Hewitson, personal communications.
17. IPCC, *2000: Special Report of the Intergovernmental Panel on Climate Change,* N. Nakicenovic, R. Swart, Eds. (Cambridge Univ. Press, Cambridge, 2000), p. 570.
18. Canadian Center for Climate Modelling and Analysis (CCCMA), model CGCM2 (www.cccma.bc.ec.gc.ca/data/cgcm2/cgcm2.shtml).
19. Commonwealth Scientific and Industrial Research Organisation (CSIRO), model Mk-2 (http://cera-www.dkrz.de/IPCC_DDC/IS92a/CSIRO/csirogcm.html).
20. Max Planck Institute for Meteorology, model ECHAM4 (www.mpimet.mpg.de/en/extra/models/echam/echam4_description.php).
21. Hadley Centre, global climate model HADCM3 (www.met-office.gov.uk/research/hadleycentre/models/HadCM3.html).
22. National Center for Atmospheric Research (NCAR), Climate System Model (CSM).
23. NCAR, Parallel Climate System Model (PCSM).
24. Model outputs for IPCC AR4 (2005) are available (https://esg.llnl.gov:8443/home/publicHomePage.do).
25. IPCC, *Special Report on Emissions Scenarios* (*SRES*) (www.grida.no/climate/ipcc/emission/098.htm).
26. A notable degree of convergence has emerged over the last decade between all of these models, both for Africa as a whole, and at large regional scales such as for southern Africa (*15*, *16*, *24*, *25*). Although individual models may disagree in specific geographic locations, in terms of area averages the multimodel mean is a good indication of the consensus change. As with all GCM simulations, care must be taken against overinterpreting fine scale information; the skill (especially with precipitation) lies in the area aggregate of the data.
27. R. Mathieu, Y. Richard, *Geophys. Res. Lett.* **32**, 10.1029/2005GL022436 (2005).
28. J. M. Bremner, J. Rogers, J. P. Willis, *Trans. R. Soc. S. Afr.* **47**, 247 (1990).
29. W. van Warmelo, *S. Afr. Irrigation* **1**, 244 (1922).
30. A decrease in precipitation, and the resulting decrease in water supply, anywhere along this band would be absolutely disastrous not just to the population in the band. Africa's two largest deltas, the Nile and the Niger, receive a substantial amount of their drainage from this unstable regime. The Nile drains 11 different countries that depend on it in varying degrees. With increasing populations and decreasing water supply, conflicts over shared water are inevitable. The fact that most models predict an increase in rainfall in East Africa does not decrease the seriousness of this problem, and, if the some of the GCMs turn out to be the correct forecast [e.g., (*20*)], the entire Nile basin, including the Sudd swamps, will be very seriously affected.
31. GraphPad Prism 4, GraphPad Software (www.curvefit.com).
32. World Climate (www.worldclimate.com).

33. Our Africa research is funded by the Africa Exploration Unit of De Beers. We thank M.C.J. de Wit of the Africa Exploration Unit for providing us with African river and climate data; D. Rothman and D. Turcotte for their interest in our African River basin analyses and for sharing their expertise on river networks, F. Cotterill for stimulating our interests in watersheds of sub-Saharan Africa, and J. Rogers for sharing knowledge on the Orange River. We have benefited in particular from discussions with B. Hewitson, who also made available to us the results of the CSAG and facilitated early access to the IPCC data bank of global climate models. We acknowledge the international modelling groups for providing their data for analysis, the Program for Climate Model Diagnosis and Intercomparison (PCMDI) for collecting and archiving the model data, the Joint Scientific Committee (JSC) of the Climate Variability (CliVar) Scientific Steering Group on Coupled Modelling (WGCM) and their Coupled Model Intercomparison Project (CMIP) and the Climate Simulation Panel for organizing the model data analysis activity, and the IPCC WG1 TSU for technical support. The IPCC Data Archive at Lawrence Livermore National Laboratory is supported by the Office of Science, U.S. Department of Energy. We thank B. Hewitson for reviewing this paper. This is AEON contribution 002.

Supporting Online Material

www.sciencemag.org/cgi/content/full/1119929/DC1
Materials and Methods
Figs. S1 to S4

8 September 2005; accepted 21 February 2006
Published online 2 March 2006;
10.1126/science.1119929
Include this information when citing this paper.

Kaposi's Sarcoma–Associated Herpesvirus Fusion-Entry Receptor: Cystine Transporter xCT

Johnan A. R. Kaleeba and Edward A. Berger*

Kaposi's sarcoma–associated herpesvirus (KSHV, human herpesvirus 8) is the causative agent of Kaposi's sarcoma and other lymphoproliferative syndromes often associated with HIV/AIDS. Functional complementary DNA selection for a receptor mediating KSHV cell fusion identified xCT, the 12-transmembrane light chain of the human cystine/glutamate exchange transporter system x_c^-. Expression of recombinant xCT rendered otherwise not susceptible target cells permissive for both KSHV cell fusion and virion entry. Antibodies against xCT blocked KSHV fusion and entry with naturally permissive target cells. KSHV target cell permissiveness correlated closely with endogenous expression of xCT messenger RNA and protein in diverse human and nonhuman cell types.

KSHV is etiologically linked to Kaposi's sarcoma and other lymphoproliferative syndromes that occur more frequently in immunocompromised individuals, including those with HIV/AIDS (*1*). Entry of herpesviruses into host cells generally occurs via attachment to the cell surface, followed by direct fusion between the virion and target cell plasma membranes; alternative routes involving receptor-mediated endocytosis have been reported in some cases (*2*). KSHV can infect a broad range of adherent cell types of different species and tissue lineages in vitro, which indicates broad distribution of the host cell components associated with virus entry; however, the outcome is almost always latency rather than productive infection (*3*). Cells expressing recombinant KSHV glycoproteins undergo cell fusion (*4*); this provides support for a direct fusion entry mechanism. Consistent with these infectivity and fusion studies, we have found that a wide range of cell types from diverse tissues and species are permissive for KSHV glycoprotein–mediated cell fusion and virion entry (*5*); we hypothesized that these processes require a specific KSHV fusion-entry receptor(s) on the target cell surface, distinct from molecules previously implicated in the attachment and entry process.

For KSHV receptor identification, we adapted a vaccinia-based cell fusion assay in which "effector" cells expressing surface viral glycoprotein(s) (and infected with a recombinant vaccinia virus encoding bacteriophage T7 RNA polymerase) were mixed with "target" cells expressing the relevant surface receptor(s) (and containing the *Escherichia coli LacZ* gene linked to the T7 promoter, introduced by plasmid transfection or recombinant vaccinia virus infection); β-galactosidase (β-gal) activity provides a quantitative measure of cell fusion (*6*). Our functional strategy for KSHV receptor identification (*7*) made no assumptions about the specific viral or cellular molecules involved but, instead, relied on the notion that a receptor-encoding cDNA within a library derived from a fusion-permissive cell line would confer fusion susceptibility to an otherwise nonpermissive target cell; use of a selectable reporter would enable enrichment of the fused cells containing the desired cDNA. As KSHV nonpermissive fusion targets, F515 or NIH 3T3 murine fibroblasts were transfected with plasmid pJK7-T7Beacon containing the T7 promoter linked to a tripartite reporter cassette encoding surface epitope tags from influenza virus hemagglutinin (HA) and Myc, plus cytoplasmic enhanced green fluorescence protein (EGFP) (fig. S1A). The targets were also infected with Mel-dT2 (fig. S1B), a

Laboratory of Viral Diseases, National Institute of Allergy and Infectious Diseases (NIAID), National Institutes of Health, Bethesda, MD 20892, USA.

*To whom correspondence should be addressed. E-mail: edward_berger@nih.gov